Coprecipitated Enzyme Encapsulated Covalent Organic Frameworks for Biocatalysis

Satyadip Paul,[1*,#] Mani Gupta,[3#] Shayan Karak,[1] Yogeshwar D. More,[7] Soumyadeep Saha,[1] Ashok Kumar Mahato,[1] Ekta Nehra,[5] Yusuke Nishiyama,[5] Jin-Chong Tan,[7*] Supratim Datta,[2,3,4*] Rahul Banerjee[1,2,6*]

[1]Department of Chemical Sciences, Indian Institute of Science Education and Research, Kolkata, Mohanpur 741246, India.

[2]Centre for Advanced Functional Materials, Indian Institute of Science Education and Research, Kolkata, Mohanpur 741246, India.

[3]Department of Biological Sciences, Indian Institute of Science Education and Research Kolkata, Mohanpur 741246, India.

[4]Center for the Climate and Environmental Studies, Indian Institute of Science Education and Research Kolkata, Mohanpur 741246, India.

[5]JEOL Ltd., Tokyo 196-8558, Japan.

[6]College of Science, Korea University, 145 Anam-ro Seongbuk-gu, South Korea.

[7]Multifunctional Materials & Composites (MMC) Laboratory, Department of Engineering Science, University of Oxford, Parks Road, Oxford OX1 3PJ, United Kingdom.

ABSTRACT: Enzymes are powerful biocatalysts but suffer from instability under extreme physiological conditions. Covalent organic frameworks (COFs) have emerged as promising supports for enzyme immobilization, enhancing both stability and reusability. In this study, we developed a one-pot aqueous synthesis method for enzyme-encapsulated COFs and provided a detailed analysis of enzyme-COF interactions. We successfully encapsulated *β*-glucosidase (BGL), alkaline phosphatase (ALP), and eight other enzymes and proteins within the TpAzo COF. Solid-state 2D NMR correlation spectroscopy, provided direct molecular-level evidence of interactions between enzyme residues and the COF backbone, confirming structural integrity and encapsulation efficiency. Scattering-type scanning near-field optical microscopy (s-SNOM) and nanoscale Fourier-transform infrared spectroscopy (nanoFTIR) further validated the presence of BGL within the COF. The encapsulated BGL and ALP retained their catalytic activity with excellent recyclability for up to ten cycles. Notably, the COF significantly enhanced BGL's stability against denaturation in aqueous sodium dodecyl sulfate (SDS) solutions across a concentration range of 1–15% (w/v). This work establishes a robust strategy for enzyme encapsulation, leveraging enzyme-COF interactions to improve stability under extreme conditions.

INTRODUCTION

Enzymes are biocatalysts with high selectivity and efficiency, making them highly valuable for industrial applications.[1-3] However, their practical use is often hindered by instability, narrow operating conditions, and challenges in recyclability.[4,5] To address these limitations, enzyme immobilization on solid materials has emerged as a promising approach to enhance enzyme stability and reusability.[6-10] Conventional immobilization materials, such as carbon, cellulose derivatives, magnetic nanoparticles, mesoporous silica, and polystyrene derivatives, have been explored.[11-17] However, these materials often suffer from drawbacks such as irregular sizes, lack of functional groups, poor porosity, and enzyme leaching.[18,19]

Porous materials like covalent organic frameworks (COFs), metal-organic frameworks (MOFs), and hydrogen-bonded organic frameworks (HOFs) offer significant advantages, including high surface areas, tunable pore environments, and enhanced stability.[20-29] While MOFs and HOFs have demonstrated potential, their applications are often limited by issues such as metal ion leaching and poor water stability. In contrast, covalent organic frameworks (COFs) are crystalline, porous materials that are metal-free and exhibit excellent thermal and chemical stability.

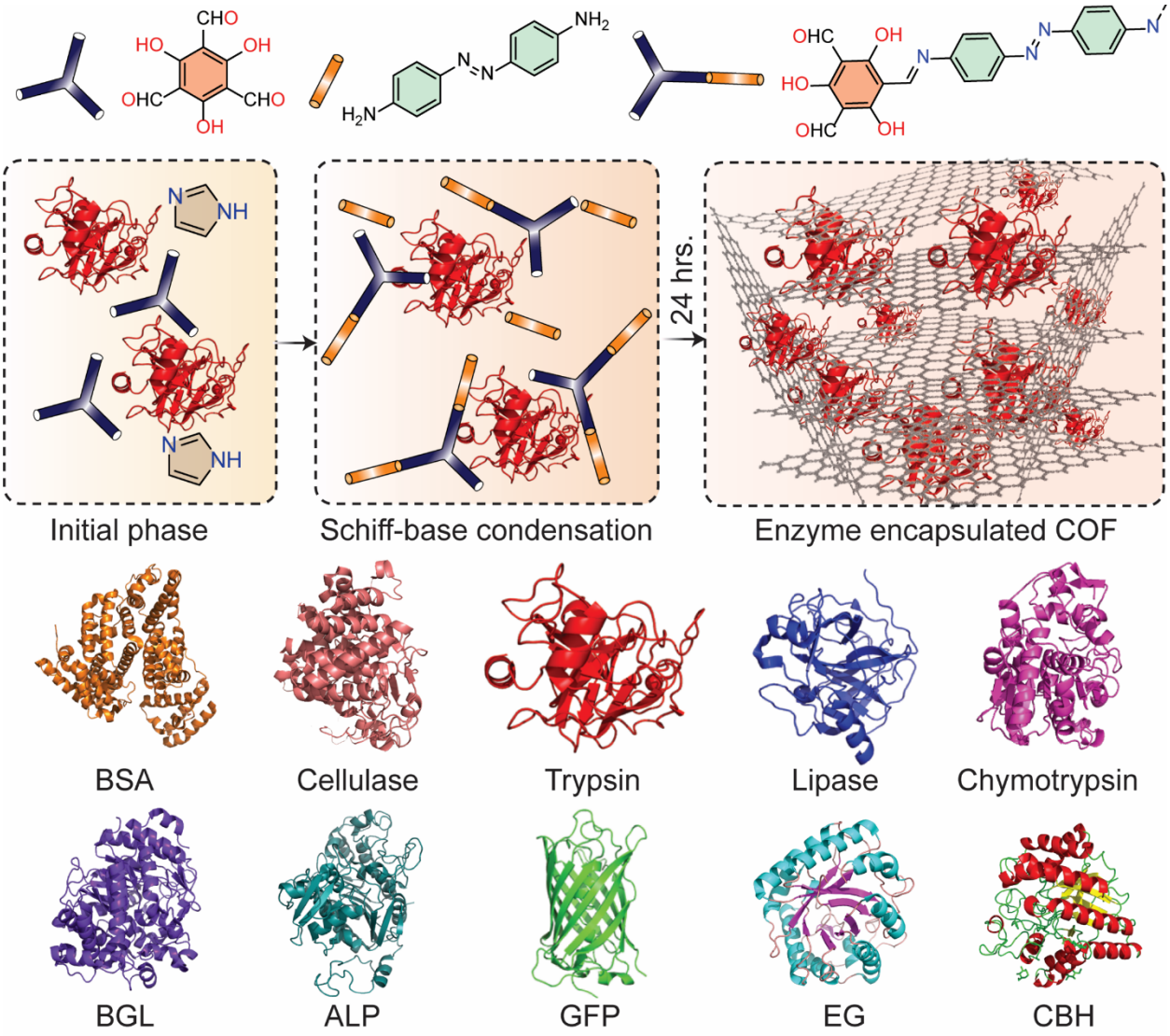

Figure 1: Schematic of the one-pot synthesis of the enzyme-encapsulated covalent organic framework (Inside the dotted box: C_3 dark blue linker represents 1,3,5-triformylpholoroglucinol (Tp), C_2 orange linker represents 4,4-azodianiline(Azo). Bottom: The figures are representative of the class of proteins and enzymes used in this study and not of the individual enzyme or protein used.

Furthermore, COFs remain stable in aqueous environments, offering a more biocompatible alternative with improved control over the microenvironment.[30,31] Despite these advantages, effective enzyme encapsulation in COFs remains a challenge due to factors such as size mismatch between enzyme molecules and COF pores, harsh synthesis conditions, and difficulty in achieving uniform enzyme distribution.[32-39]

A critical aspect of enzyme-encapsulated COFs is their proper characterization, essential for understanding the enzyme-COF interactions, encapsulation efficiency, and structural stability. However, current characterization techniques face several challenges. Conventional spectroscopic and diffraction methods, such as Fourier-transform infrared (FTIR) spectroscopy, powder X-ray diffraction (PXRD), and thermogravimetric analysis (TGA), often fail to provide direct evidence of enzyme encapsulation at the molecular level.[37] Additionally, the inherent complexity and heterogeneity of enzyme-COF composites make it difficult to distinguish between physically adsorbed and, indeed, encapsulated enzymes. The presence of multiple functional groups in both the COF framework and the enzyme further complicates the spectral interpretation.

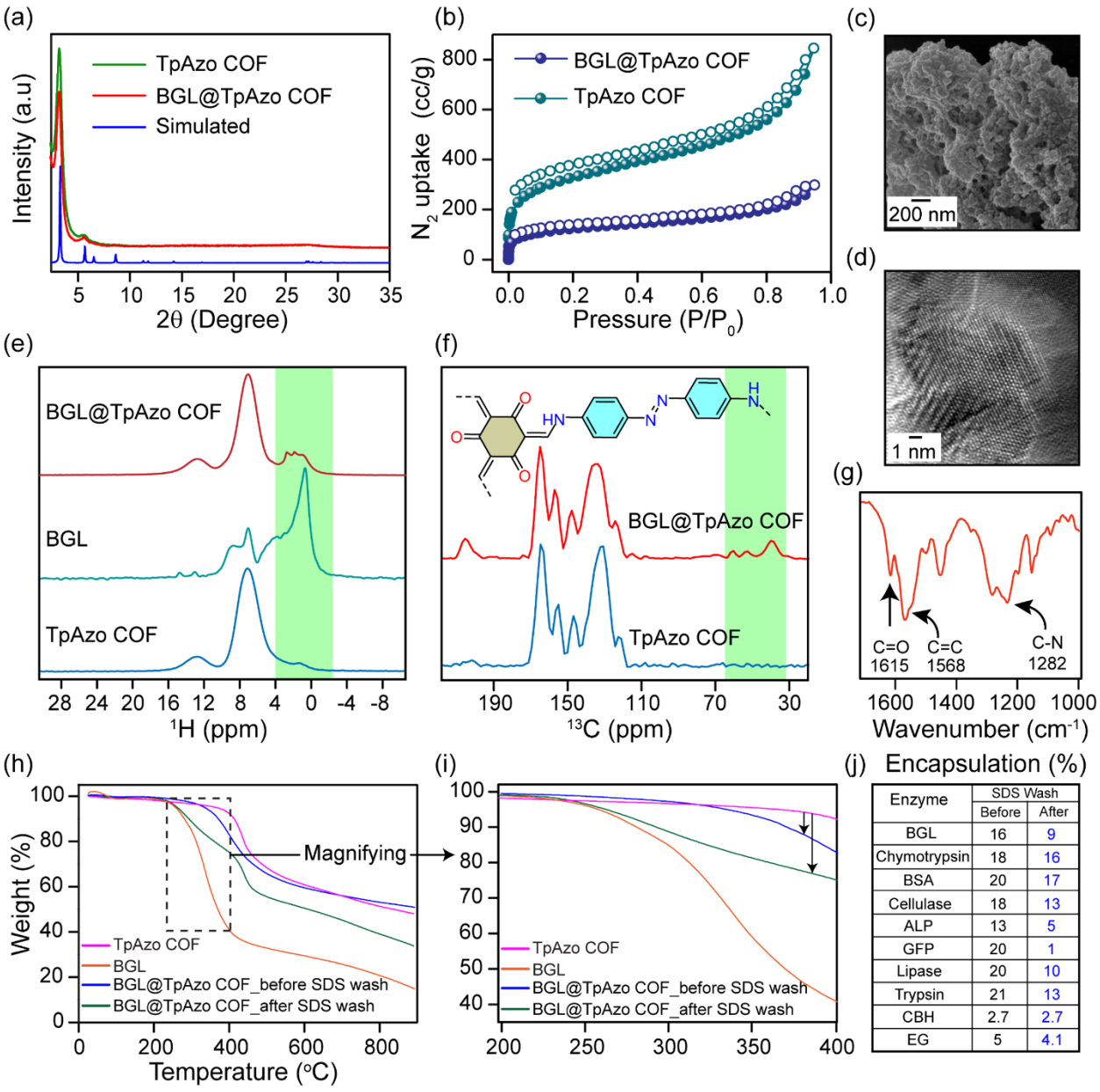

Enzyme	SDS Wash	
	Before	After
BGL	16	9
Chymotrypsin	18	16
BSA	20	17
Cellulase	18	13
ALP	13	5
GFP	20	1
Lipase	20	10
Trypsin	21	13
CBH	2.7	2.7
EG	5	4.1

Figure 2: (a) Powder X-ray diffraction (PXRD) of TpAzo COF and BGL@TpAzo COF. (b) N_2 adsorption isotherms of TpAzo COF and BGL@TpAzo COF. (c) SEM (d) TEM image of BGL@TpAzo COF. (e) Solid-state ^{1}H NMR of BGL, TpAzo COF, and BGL@TpAzo COF. (f) Solid-state ^{13}C NMR of TpAzo COF and BGL@TpAzo COF. (g) FT-IR spectra of TpAzo COF. (h) TGA curve of TpAzo COF, BGL, BGL@TpAzo COF before and after SDS wash. (i) Magnified portion of TGA curves between 200 to 400 °C. (j) List of encapsulation percentages of all the enzymes before and after SDS (10% w/v) wash.

Moreover, commonly used enzyme activity assays only provide indirect evidence of encapsulation and do not elucidate the structural integrity of the enzyme within the COF.[41]

To overcome these limitations, advanced characterization techniques such as solid-state 2D nuclear magnetic resonance (NMR) spectroscopy, scattering-type scanning near-field optical microscopy (s-SNOM), and nanoscale Fourier-transform infrared spectroscopy (nanoFTIR) have been employed.[42-45] These methods enable direct visualization of enzyme-COF interactions at the molecular level and provide high-resolution structural insights. Here, we developed an aqueous synthesis method that allows enzyme encapsulation under ambient conditions, preserving enzyme integrity while forming stable COF structures.

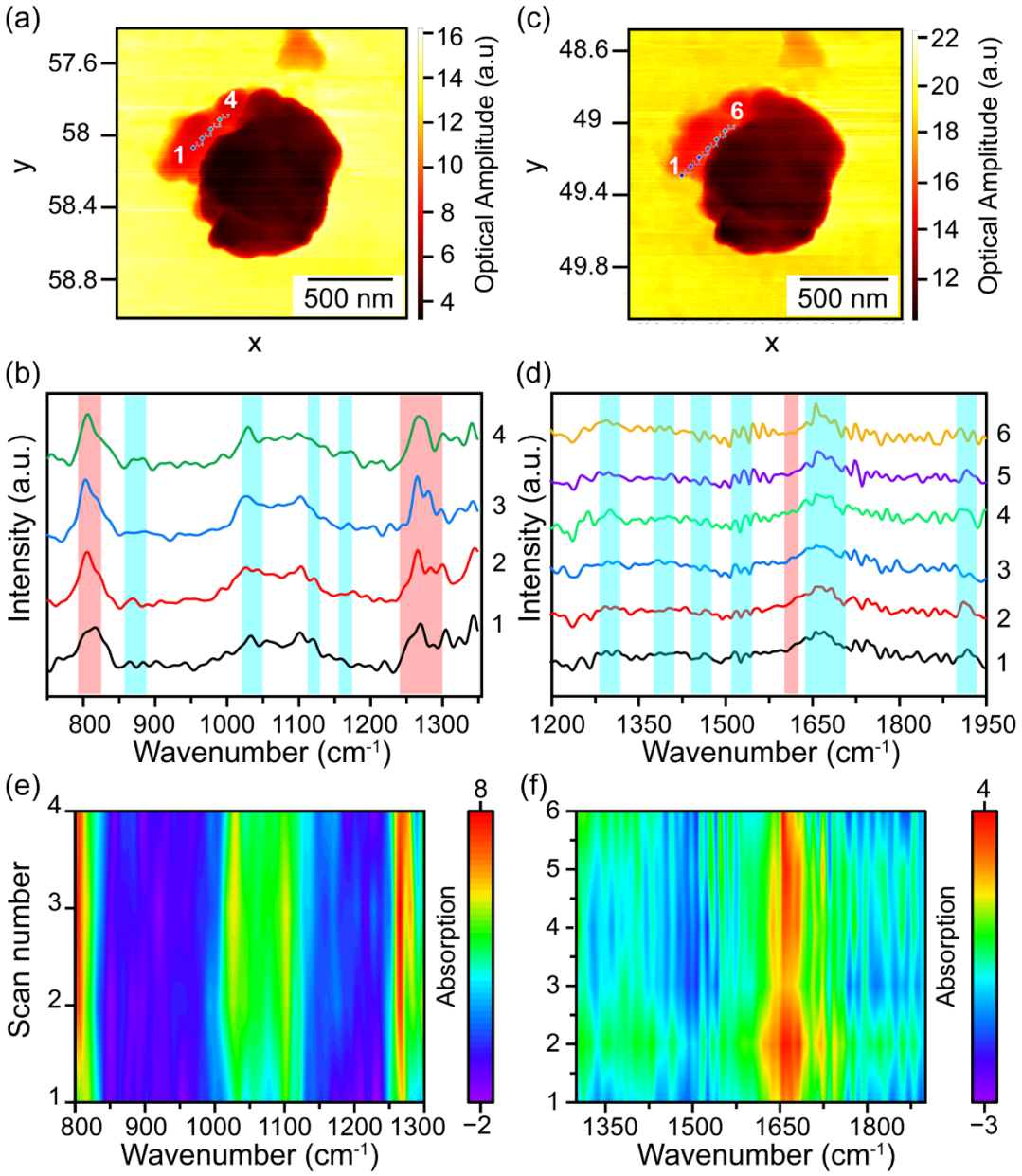

Figure 3: s-SNOM infrared imaging (Near-field optical spectroscopy) of individual nanocrystals of exposed BGL@TpAzo COF. (a) A white light optical amplitude image for BGL@TpAzo COF treated nanocrystal. (b) Near-field mid-IR spectra of BGL@TpAzo COF nanocrystals were obtained via nanoFTIR multi-point line scans, which measured points 1-4 under laser A region (650-1350 cm^{-1}). (c) Optical amplitude image for BGL@TpAzo COF nanocrystals. (d) Near-field mid-IR spectra of BGL@TpAzo COF nanocrystals obtained via nanoFTIR multi-point line scans measurements for points 1-6 under Laser C region (1350 – 2250 cm^{-1}). (e) nanoFTIR contour plots were obtained with Laser A to prove the BGL@TpAzo COF nanocrystals. (f) nanoFTIR contour plots were obtained with Laser C probing BGL@TpAzo COF nanocrystals (Green, yellow, and red color zones indicate incremental absorption intensity).

We designed a one-pot biomineralization-inspired methodology wherein enzymes self-assemble with COF linkers during synthesis, leading to the co-precipitation of enzyme@COF composites. The application of 2D solid-state NMR, s-SNOM, and nanoFTIR confirmed the presence of enzymes within the COF matrix and their stable interactions.

The encapsulated enzymes, such as *β*-glucosidase (BGL) and alkaline phosphatase (ALP), demonstrated efficient catalytic activity and recyclability while maintaining stability in harsh conditions, such as exposure to a 1-15% aqueous SDS solution. Beyond these two enzymes, our strategy also enabled the encapsulation of eight other enzymes and proteins, such as cellobiohydrolase (CBH), endoglucanase (EG),

cellulase, trypsin, chymotrypsin, bovine serum albumin (BSA), and green fluorescent protein (GFP), showcasing the versatility and potential of COFs as robust hosts for biocatalysis.

RESULTS AND DISCUSSION:

The keto-enamine-based TpAzo COF was chosen as the model host carrier owing to its higher surface area, stability, crystallinity, and structural integrity. Guo et al. previously reported the synthesis of covalent organic frameworks using imidazole.[46] Following this methodology, we fabricated the enzyme-encapsulated TpAzo COF in the presence of imidazole. Imidazole plays a crucial role in the formation of the COF by facilitating the dissolution of monomers, such as the aldehyde and amine, in water. This is due to imidazole's ability to form hydrogen bonds, as it possesses both hydrogen bond donor and acceptor sites. Furthermore, its weakly acidic nature catalyzes the Schiff base reaction between the aldehyde and amine groups, leading to the formation of the COF. The enzyme-encapsulated COF was synthesized in an aqueous medium at room temperature. Typically, 0.05 mmol of 1,3,5-triformylpholoroglucinol (Tp), 0.075 mmol of 4,4-azodianiline (Azo), 0.5 mmol of imidazole, and 1 mg of enzyme or protein were added in 1 mL Mili-Q water in a 10 mL glass vial. The mixture was allowed to stir for 24 hours (Figure 1). During this process, the enzyme starts assembling with the linkers and self-assembles during the condensation (imine to enamine) of the linkers, resulting in the co-precipitation of the enzyme-encapsulated COF (Figure 1). The as-synthesized precipitate was repeatedly washed with water and then with 10 % aqueous SDS solution. The enzyme-encapsulated COF was thoroughly rinsed again with Milli-Q water several times to ensure the removal of any residual SDS molecules from the surface of the enzyme-encapsulated COF matrix and was dried by freeze drying for further characterization. This methodology was used on enzymes and proteins such as BGL, CBH, EG, ALP, proteases, BSA, lipase, cellulase, and GFP to synthesize enzyme-encapsulated COFs. We selected BGL-encapsulated COF for further characterization. The powder X-ray diffraction (PXRD) patterns of TpAzo COF and BGL@TpAzo COF show a diffraction peak at 3.2° (2Θ) corresponding to diffraction from the (100) planes and another peak at 5.6° (2Θ) corresponding to the diffraction from (110) planes (Figure 2a). These PXRD patterns affirm the crystalline nature and the presence of an ordered channel in the TpAzo COF. Brunauer-Emmett-Teller (BET) surface area of the as-synthesized TpAzo COF is 1180 $m^2 g^{-1}$ (Figure 2b). Non-local density functional theory (NLDFT) shows the porosity of the COF centered at 1.3 nm (Figure S2). N_2 adsorption measurement of BGL@TpAzo COF shows a type-I isotherm and BET surface area of 450 $m^2 g^{-1}$ and pore size distribution centered at 1.3 nm (Figure 2b). The reduction of the surface area is due to the occupancy by BGL. Time-dependent scanning electron microscopy (SEM) images exhibit the stepwise assembly of COF crystallites with the enzymes for encapsulation. After six hours, we observed the formation of randomly oriented COF crystallites and the presence of BGL (Figure S3). Gradually, these crystallites started assembling into sheet-like structures, encapsulating the BGL (Figure S2). Finally, the assembled structures of BGL-encapsulated COF sheets were co-precipitated (Figures 2c and S3). Lattice fringes in the high-resolution transmission electron microscopy (HR-TEM) images of the BGL@TpAzo COF reveal the crystalline porous nature of the composite. (Figures 2d and S4). Solid-state ^{1}H NMR affirms the presence of BGL in TpAzo COF. The spectra were observed after DQ (double quantum) filtering to suppress ^{1}H signals of residual solvent, highlighting the rigid BGL and COF signals (Figure 2e). ^{1}H solid-state NMR of TpAzo COF shows the presence of aromatic protons in the region from $\delta_H \simeq$ 5-9 ppm and -N–H protons around $\delta_H \simeq$ 13 ppm. ^{1}H solid-state NMR of free BGL shows two kinds of peaks. Aromatic and amide proton signals appear between $\delta_H \simeq$ 5-10 ppm, and aliphatic protons (α ^{1}Hs and β ^{1}Hs) fall in the region of $\delta_H \simeq$ 0-4 ppm (Figure 2e). Consequently, ^{1}H solid-state NMR of BGL@TpAzo COF shows an additional signal in the region $\delta_H \simeq$ 0-4 ppm arising from the α and β ^{1}Hs of BGL encapsulated in TpAzo COF (Figure 2e). Solid-state ^{13}C NMR spectra of TpAzo COF and BGL@TpAzo COF were taken from ^{13}C projection of 2D ^{13}C-^{1}H correlation spectra. ^{13}C NMR spectrum of TpAzo COF shows the presence of aromatic carbon in the region of $\delta_{13C} \simeq$ 110-160 ppm. In addition to aromatic carbons, BGL@TpAzo COF exhibits ^{13}C NMR peaks at $\delta_{13C} \simeq$ 30-70 ppm, which indicates the presence of aliphatic carbon, thus BGL, in the TpAzo COF (Figure 2f). Fourier-transform infrared spectroscopic (FT-IR) analysis of TpAzo COF shows the characteristic peaks at 1615 cm^{-1} (—C═O), 1568 cm^{-1} (—C═C—), and 1282 cm^{-1} (C—N) (Fig. 2g). All these characteristic peaks affirm the *β*-ketoenamine structure of the COF backbone. The thermogravimetric analysis (TGA) curve affirms the thermal stability of TpAzo COF up to a temperature of 400 ˚C (Figure 2h). The TGA curve of free BGL shows the degradation of BGL in the region from 200 to 400 ˚C. TGA curves of BGL@TpAzo COF before and after SDS (10% w/v) wash show a deeper fall compared to the pristine COF, corresponding to the percentage of BGL encapsulated in the COF (Figures 2h and 2i). The percentages (wt/wt) of encapsulated BGL before and after SDS wash are 16% and 9%, respectively. SDS disrupts both the intramolecular and intermolecular

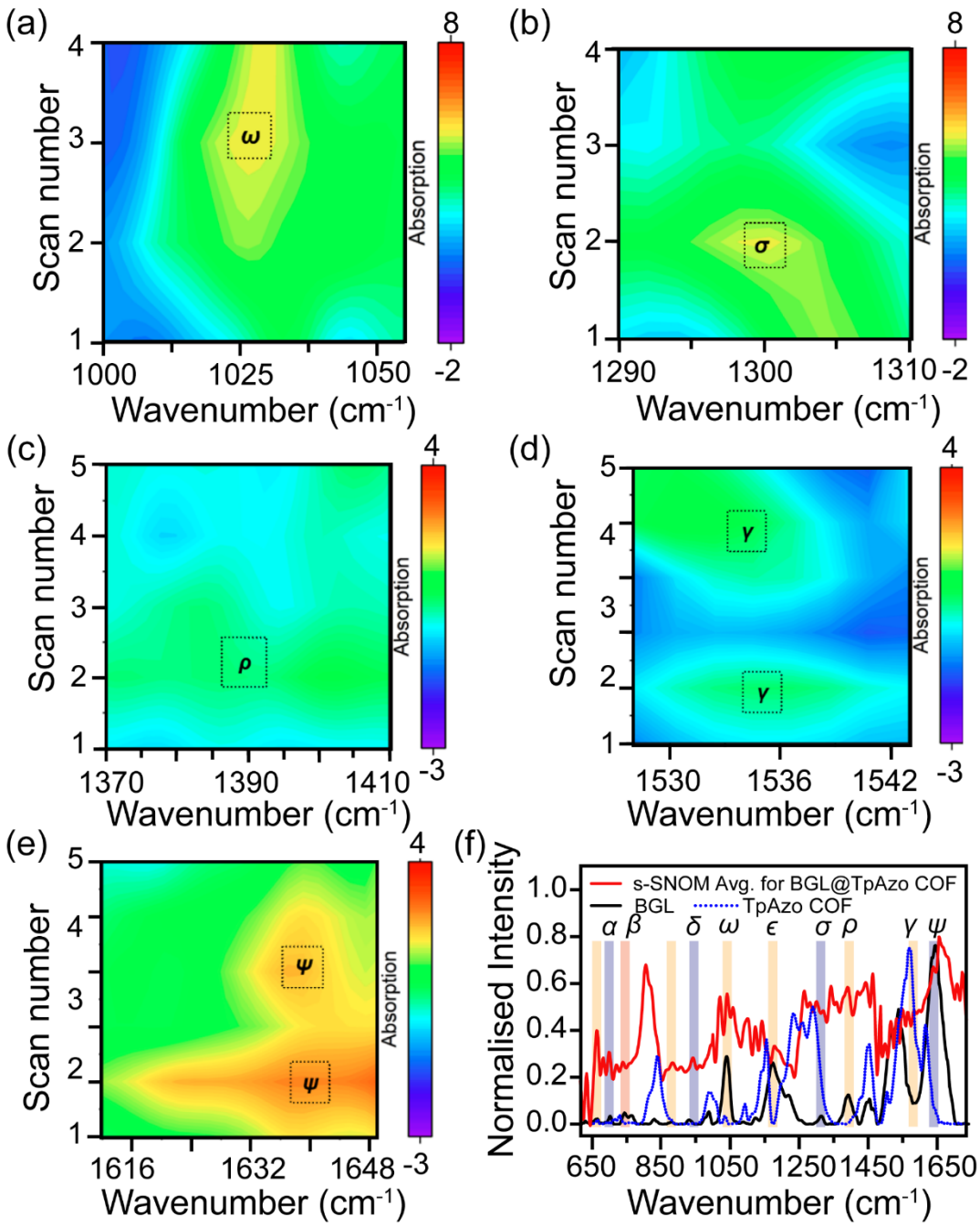

Figure 4: (a-e) nanoFTIR derived resolved 3D absorption contour plots obtained for BGL encapsulated COF (BGL@TpAzo COF) nanocrystals revealing BGL embodiment for distinctive absorption peaks at ω (1042 cm^{-1}), σ (1301 cm^{-1}), ρ (1390 cm^{-1}), γ (1537 cm^{-1}), ψ (1640 cm^{-1}). (f) Comparison of averaged (Avg.) near-field mid-IR spectra of BGL@TpAzo COF nanocrystals (red spectrum) obtained via nanoFTIR multi-point line scans measurements combining laser A and laser C with that of the enzyme (BGL; black spectrum) and TpAzo COF alone (dotted spectrum, blue spectrum).

non-covalent interactions of enzymes and the interactions between the enzyme and COF surfaces.[47] This causes the detachment of the surface-attached enzymes. Following this methodology, we screened nine other enzymes and proteins, namely CBH, EG, chymotrypsin, BSA, cellulase, ALP, GFP, lipase, and trypsin, to validate this methodology. Encapsulation percentages (wt/wt) of CBH, EG, chymotrypsin, BSA, cellulase, ALP, GFP, lipase, and trypsin before SDS wash are 2.7, 5, 18, 20, 18, 13, 20, 20, and 21%,

respectively (Figures 2j and S16) and after SDS wash are 2.7, 4.1, 16, 17, 13, 5, 1, 10, 13%, respectively (Figures 2j and S17).

The use of near-field infrared nanospectroscopy for investigating frameworks related to stabilization and guest confinement phenomena is becoming established in the literature.[43-45] In order to prove the encapsulated BGL in the TpAzo framework and find spectral features for both pristine COF and BGL@TpAzo COF, s-SNOM and nanoFTIR were performed. Well-dispersed and consistently prepared crystal domains, ranging down to the nanometer scale, were utilized for s-SNOM (scattering-type scanning near-field optical microscopy) studies (Figure S7). The nanocrystals displayed distinct geometric features characterized by smooth edges and flake-like morphologies (Figures 3a and 3c). Simultaneous nanoFTIR (nanoscale Fourier-transform infrared) spectroscopy of BGL@TpAzo COF exhibited a consistent peak pattern in the mid-infrared region. Notable absorption bands were observed at 840, 1263, 1287, and 1616 cm^{-1}, originating from the TpAzo COF backbone. Additionally, characteristic peaks at 1038, 1120, 1172, 1315, 1414, and 1453 cm^{-1} were attributed to the encapsulated BGL. The presence of BGL was further confirmed by absorption bands in the amide-II region[48] (1514, 1539, 1540, 1549, and 1570 cm^{-1}) and the amide-I region[45] (1645, 1659, 1668, and 1682 cm^{-1}) (Figures 3b and 3d). These peaks closely matched the ATR-FTIR far-field spectral features (Figures S5 and S6a) and exhibited the composite nature of the material (Figures 3f and S5). The distinctive vibrational bands, representing features of both the host framework (COF) and the guest enzyme, were further observed in 3D contour plots (Figures 3e and 3f). These plots were derived from near-field measurements using Laser A and Laser B over uniformly scanned regions and multiple points along the sample line (BGL@TpAzo COF).

These observations are further confirmed by multiple point scans performed across the pristine and composite samples (Figures S7-S10). This study also demonstrates the stability of BGL@TpAzo COF towards heat treatment (90-100 °C). BGL@TpAzo COF retaining its framework after baking at 90–100 °C and subsequent humidity exposure. Structural integrity was confirmed by point scan analysis along the nanocrystals (Figures 3a–3d).

The resolved analysis of 3D contour plots (Figures 4a-4e) and the averaged spectra of the composite BGL@TpAzo COF, alongside the IR bands of the guest enzyme (BGL, black spectrum) and the host COF, suggests that the composite exhibits strong IR absorption bands in the mid-IR region (Figure 4f). These bands include characteristic peaks from the host and guest moieties. The host, being present in bulk, is expected to exhibit prominent features. However, a closer examination of the 3D contour plots obtained via the s-SNOM technique reveals distinctive absorption bands corresponding to the loaded guest motifs at specific frequencies: ω (1042 cm^{-1}), σ (1301 cm^{-1}), ρ (1390 cm^{-1}), γ (1537 cm^{-1}), and ψ (1640 cm^{-1}) (Figures 4a-4e, respectively). The absence of ω, σ, ρ, γ, and ψ bands in TpAzo COF, their exclusive presence in BGL, and their manifestation in BGL@TpAzo COF indicate composite characteristics. This observation aligns with the far-IR spectral features revealed in the second derivative analysis of BGL (Figure S6b). These observations confirm the successful loading and prominent presence of the enzyme (guest) within the host framework. The findings from the s-SNOM technique were further validated using far-field infrared spectroscopic measurements conducted on the composite nanoparticles within the measurement range of 650 cm^{-1} to 2000 cm^{-1}. These measurements were compared with pristine COF particles, which exhibited nanometer to micrometer-scale thickness (Figures S9 and S10). Both samples were subjected to controlled humidity exposure to replicate the conditions used in the s-SNOM analysis.

We performed a series of ^{1}H double quantum (DQ)-^{1}H single quantum (SQ) homonuclear and ^{13}C-^{1}H heteronuclear correlation solid-state NMR experiments to probe the interatomic proximities within approximately 4 Å, thereby confirming encapsulation of BGL with the TpAzo COF scaffold. ^{1}H DQ frequency corresponds to the sum of the ^{1}H chemical shifts of two interacting protons, and the ^{1}H SQ frequency is determined by the chemical shifts of individual protons. All peaks observed in TpAzo COF and BGL align with their respective molecular structures (Figures 5a-5f). Owing to the high MAS rate of 70 kHz, the ^{1}H NMR spectra exhibit high-resolution peaks. ^{1}H peaks around 8 ppm are present in TpAzo COF and BGL, corresponding to aromatic and amide protons, respectively. Additionally, distinct peaks appear at 13 ppm for TpAzo COF (—N—H protons) and 0-2 ppm for BGL (α and β protons). The intramolecular correlations at (^{1}H DQ, ^{1}H SQ) = (20 ppm, 7/13 ppm) in TpAzo COF and (10 ppm, 2/8 ppm) in BGL corroborate these spectral assignments. Furthermore, ^{13}C-^{1}H correlation spectra confirm the presence of aromatic correlations at (^{13}C, ^{1}H) = (110-150 ppm, 8 ppm) in TpAzo COF and the correlation of α/β CH at (^{13}C, ^{1}H) = (20/60 ppm, 1/5 ppm) in BGL. All of these correlation peaks are also observed in

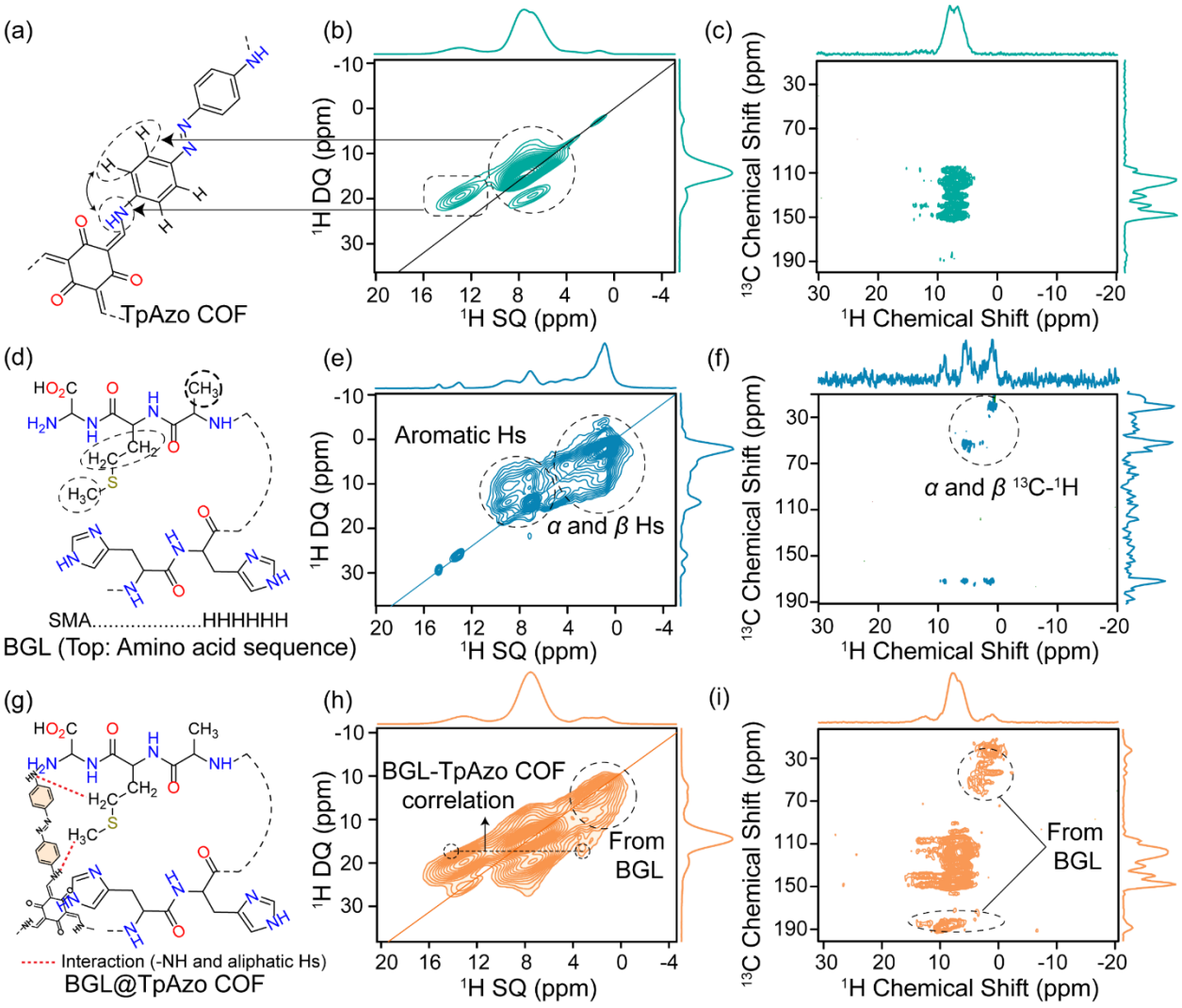

Figure 5: (a) Structure of TpAzo COF. (b) ^{1}H-^{1}H DQ-SQ spectra of TpAzo COF. (c) ^{1}H-^{13}C double CP spectra of TpAzo COF. (d) Structure of BGL. (e) ^{1}H-^{1}H DQ-SQ spectra of BGL. (f) ^{1}H-^{13}C double CP spectra of BGL. (g) Structure of BGL@TpAzo COF. (h) ^{1}H-^{1}H DQ-SQ spectra of BGL@TpAzo COF. (i) ^{1}H-^{13}C double CP spectra of BGL@TpAzo COF.

BGL@TpAzo COF spectra (Figures 5h and 5i), indicating the existence of TpAzo COF and BGL within the BGL@TpAzo COF framework. More importantly, a closer look at the (^{1}H DQ, ^{1}H SQ) correlation spectrum of BGL@TpAzo COF reveals intermolecular proximity between α/β protons of BGL and NH protons of TpAzo COF at (^{1}H DQ, ^{1}H SQ) = (15-18 ppm, 2-5 ppm), further supporting the encapsulation of BGL within the TpAzo COF framework (Figures 5g and 5h). Additionally, the identical spectral patterns observed in ^{1}H DQ-^{1}H SQ and ^{13}C-^{1}H spectra confirm the structural integrity of the COF scaffold in BGL@TpAzo COF. The same analysis was conducted for ALP@TpAzo COF (Figure S12), where the intermolecular correlation between α/β protons of ALP and N—H protons of TpAzo COF strongly supports the encapsulation of ALP within the TpAzo COF framework. While no clear intermolecular correlations were observed in chymotrypsin@TpAzo COF (Figure S13), the spectral patterns confirm the coexistence of chymotrypsin and TpAzo COF.

We performed a 3D confocal laser scanning microscopic image (CLSM) experiment using a labeled FITC (Fluorescein isothiocyanate) enzyme. 3D CLSM was executed before and after the wash of FITC-Enzyme@COF with 10% SDS. The intense fluorescent signal from the green channel before the SDS wash affirms the presence of FITC-BGL in TpAzo COF (Figure 6a). However, the fluorescence intensity of the green channel drops after the SDS wash, as surface-adsorbed FITC-BGL washed away (Figure 6b). Similarly, EG was labeled with FITC, and CLSM was performed with the as-synthesized FITC-EG@TpAzo COF before and after 10 % SDS wash. The fluorescence intensity of the green signal before and after 10% SDS

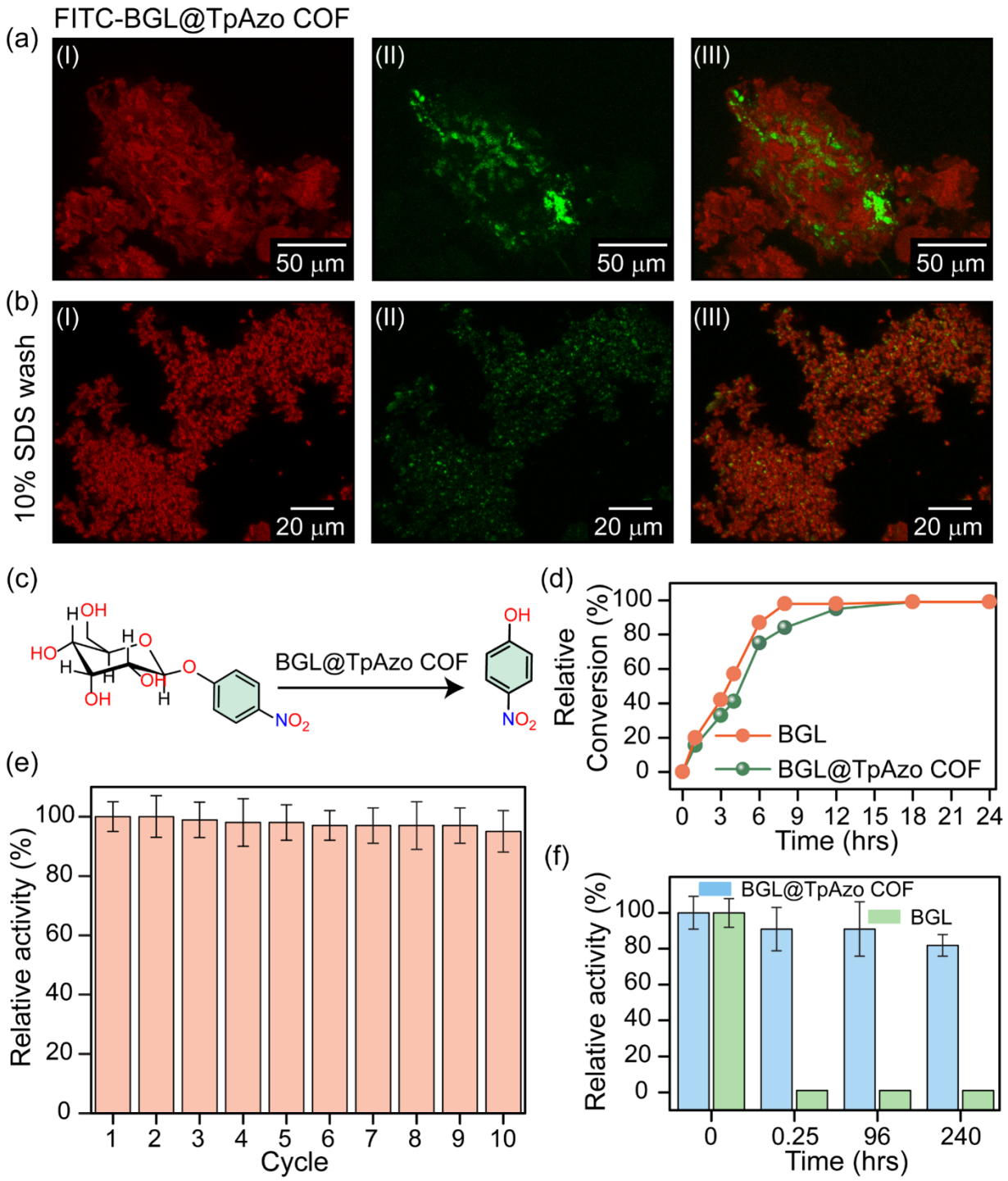

Figure 6: Confocal microscopy images of FITC-labeled BGL (FITC-BGL) encapsulated in TpAzo COF before and after SDS wash (a) Before SDS wash: (I) TpAzo COF, (II) FITC-BGL, (III) merged overlay of I and II. (b) After SDS wash: (I) TpAzo COF. (II) FITC-BGL (III) overlay of I and II. (c) Schematic diagram of BGL@TpAzo COF catalyzing the hydrolysis of *p*-nitrophenyl-*β*-D-glucopyranoside (*p*NPGlc) to *p*-nitrophenol (*p*NP). (d) Conversion kinetics of *p*NPGlc to *p*NP catalyzed by free BGL and BGL@TpAzo COF. (e) Recyclability of BGL@TpAzo COF over multiple cycles. (f) Relative enzymatic activity of free BGL and BGL@TpAzo COF in the presence of 10 % (w/v) SDS solution.

wash remained identical (Figure S14), as EG interacts strongly with the functional groups of the COF surface.[49] We also performed 3D CLSM of FITC-CBH@TpAzo COF before and after the SDS wash. The

intensity of the green channel dropped after the SDS wash (Figures S15a and S15b). These results confirm the encapsulation of FITC-CBH in the TpAzo COF. We performed 3D CLSM of the GFP@TpAzo COF. An intense green-fluorescent image before SDS wash reveals the presence of GFP in the COF matrix. However, after the SDS wash, the fluorescent signal was diminished (Figures S15c and S15d). This confirmed that SDS obliterates the GFP from the COF backbone, which is consistent with the TGA experiment that was previously performed to calculate the percentage of encapsulation of GFP before and after SDS wash. We hypothesize that GFP gets encapsulated only in the COF surface rather than inside the matrix.

We investigated the effect of imidazole on the 3D conformation of the enzyme during the enzyme-COF composite formation. We have incubated BGL in the Milli-Q water and 0.5 millimolar aqueous imidazole solution separately at room temperature for twenty-four hours. Buffer exchange was performed to remove the residual water and imidazole from the solution. We have recollected the BGL in the buffer and performed the circular dichroism (CD) experiment. We have seen identical CD spectra of BGL recovered from water and imidazole solutions, respectively (Figure S18). These spectra affirm that the tertiary structure was retained and not perturbed even after incubation in the imidazole solution. This establishes the non-denaturing property of imidazole towards BGL.

We checked the activity of the BGL encapsulated in TpAzo COF. BGL hydrolyzes the para-nitrophenyl-*β*-D-glucopyranoside (*p*NPGlc) to para-nitrophenol (*p*NP) (Figure 6c). BGL and BGL encapsulated in TpAzo COF fully convert the substrate in 21 hours (Figure 6d). We measured the recyclability of the BGL@TpAzo COF, and it retains 98% of its initial activity after ten cycles (Figure 6e). The TpAzo COF holds it's crystallinity after ten cycles (Figure S11). We measured kinetic parameters such as K_m and V_{max} of free BGL and BGL@TpAzo COF. V_{max} of free BGL and BGL-encapsulated COF are 402.1±9.2 μM min^{-1} and 277.7±7.5 μM min^{-1}. K_m of free BGL and BGL-encapsulated COF are 1.9±0.2 mM and 2 ±0.3 mM (Figure S20). These results indicate that the encapsulated enzyme retains catalytic activity upon encapsulation. Additionally, the decrease in V_{max} may reflect restricted molecular mobility or partial diffusion limitations within the COF matrix. We then checked the protecting capability of BGL@TpAzo COF. We immersed the free BGL and BGL@TpAzo COF in an SDS solution (10% w/v). Free BGL loses its specific activity completely after 0.25 hours (fifteen minutes). BGL encapsulated in TpAzo COF retains 82% specific activity after 10 days (Figure 6f). Additionally, we incubated both free BGL and BGL@TpAzo COF in the presence of SDS at different concentrations (1-15%) for two hours to assess their stability. Our results show that free BGL is highly sensitive to SDS and loses enzymatic activity even at low concentrations (1%). In contrast, BGL@TpAzo COF exhibits remarkable stability in SDS solutions, retaining 86–90% (Figure S21 and section S4) of its relative activity across various SDS concentrations. It confirms that the BGL is protected inside the COF from the denaturing agent like SDS. Also, we conducted stability experiments comparing the enzymatic activity of free β-glucosidase (BGL) and encapsulated BGL in TpAzo COF (BGL@TpAzo COF) in various organic solvents. Free BGL exhibited a complete loss of activity across all tested solvents. In contrast, BGL@TpAzo COF retained 70–90% of its initial activity in the presence of a wide range of organic solvents, including acetone, acetonitrile, dichloromethane (DCM), 1,4-dioxane, dimethyl sulfoxide (DMSO), tetrahydrofuran (THF), dimethylformamide (DMF), methanol (MeOH), hexane, and o-xylene (Figure S22 and section S4). These results highlight the enhanced solvent stability of the enzyme-encapsulated TpAzo COF matrix. Additionally, we conducted experiments to assess the long-term storage stability of free BGL and BGL encapsulated in the TpAzo COF (BGL@TpAzo COF) under ambient conditions (25 °C). Free BGL exhibited a complete loss of activity after 10 days of storage, indicating poor stability under this condition. In contrast, BGL@TpAzo COF retained approximately 75% and 73% of its initial enzymatic activity after 10 and 25 days, respectively (Figure S23). These findings clearly demonstrate that the TpAzo COF framework significantly enhances the structural and functional stability of the enzyme over extended storage periods. To identify specific interactions between BGL and the COF, we conducted ^{1}H DQ–^{1}H SQ NMR on BGL@TpAzo COF, revealing hydrogen bonding between the enzyme's Ha/Hb protons and the COF's NH groups within 4 Å (Figure 5h). In our previous work, molecular dynamics and QM/MM simulations revealed specific non-covalent interactions between BGL and the TpAzo COF-Foam.[49] The β-ketoenamine backbone of TpAzo COF, with its NH protons and oxygen atoms, serves as both a hydrogen bond donor and acceptor, enabling selective binding to complementary groups on the enzyme. Combined with NMR data, these findings confirm the presence of specific hydrogen bonding interactions between the enzyme and the COF. After BGL, we checked the activity of encapsulated ALP in the COF. ALP hydrolyses the phosphate monoester and releases the phosphate group from any organic molecule in alkaline conditions. We have taken *p*-nitrophenyl phosphate (*p*NPP) and applied ALP@TpAzo COF to produce *p*-nitrophenol (*p*NP) (Figure S19a). The ALP@TpAzo COF hydrolyzes completely within 24

hours (Figure S19b). ALP@TpAzo COF holds 97% activity after ten cycles (Figure S19c). We also compared our encapsulation strategy and characterization methods with those employed in existing enzyme immobilization approaches using alternative materials (Table S2).

CONCLUSION

In conclusion, we have developed a methodology for fabricating enzyme-encapsulated covalent organic frameworks, where COF crystallites assemble around the enzyme during growth. Using solid-state NMR, s-SNOM, and nanoFTIR spectroscopy, we have, for the first time, confirmed the presence of enzymes within the COF matrix and their interaction. Additionally, 3D CLSM provided detailed visualization of the enzyme-encapsulated COF structure. We demonstrated that BGL and ALP-encapsulated COFs retain catalytic activity and are recyclable for at least ten cycles. Moreover, BGL encapsulated in COFs exhibits greater stability than free enzymes when exposed to denaturing agents like SDS, highlighting the protective nature of the COF matrix under harsh conditions. Also, BGL encapsulated in TpAzo COF shows long-term stability under ambient conditions, unlike free BGL. We screened ten different enzymes and proteins and further validated the versatility of this methodology. This work highlights the importance of advanced characterization techniques in establishing the structural and functional integrity of enzyme@COF composites. We believe that these findings might pave the way for a sustainable and efficient approach to heterogeneous biocatalysis, offering new possibilities for enzyme stabilization and reuse in the biotechnology industry.

ASSOCIATED CONTENT

Supporting Information. Synthesis, crystallography, and characterization details are provided in the Supporting Information file. This material is available free of charge via the Internet at http://pubs.acs.org.

AUTHOR INFORMATION

Corresponding Author

* paulsatyadip105@gmail.com
* jin-chong.tan@eng.ox.ac.uk
* supratim@iiserkol.ac.in
* r.banerjee@iiserkol.ac.in

ORCID

Rahul Banerjee: 0000-0002-3547-4746
Supratim Datta: 0000-0002-8477-0058
Jin-Chong Tan: 0000-0002-5770-408X
Yusuke Nishiyama: 0000-0001-7136-1127
Ekta Nehra: 0000-0002-4779-4384
Ashok Kumar Mahato: 0000-0001-517-1598
Soumyadeep Saha: 0009-0006-7894-6105
Yogeshwar D. More: 0000-0002-0968-0220
Shayan Karak: 0000-0002-5662-6569
Mani Gupta: 0000-0003-4834-1173
Satyadip Paul: 0000-0002-1494-709X

Author Contributions

‡SP, MG contributed equally to this work. R.B. and S.D. supervised the project. S.P., M.G., S.D., and R.B. conceived and designed the project. S.P. designed all the experiments, synthesized the building blocks, performed the encapsulation studies, collected and analyzed the characterization data, and prepared all the figures. M.G. synthesized enzymes and performed experiments. S.S. assisted in the encapsulation of enzymes. Y.M. and J.-C.T. performed the nanoFTIR. E.N. and Y.N. collected and analyzed solid-state NMR. The manuscript was written through the contributions of S.P., M.G., S.K., Y.M., A.K.M., Y.N., J.-C.T., S.D., and R.B. All authors have given approval to the final version of the manuscript.

Notes

The authors declare no competing financial interests.

ACKNOWLEDGMENT

SP acknowledges CSIR for a Research fellowship. MG acknowledges DST-INSPIRE for a Senior Research Fellowship. SK acknowledges PMRF for the Senior Research Fellowship. YM and JCT thank the ERC Consolidator grant (PROMOFS grant agreement 771575) for funding. R.B. acknowledges the the funding from the DST Project; DST/C3E/MI2.0/CCUS/2K23/CALL/2023/153, submitted against FOA R&D in the area of CCUS with Mission Innovation.. SD acknowledges SERB Core Research Grant (CRG/2023/002111), and DBT, Government of India (grant number BT/PR47801/BCE/8/1812/2023). We acknowledge Mr. Ritabrata Ghosh for the confocal data collection. We acknowledge Mr. Anshuman Das for his assistance in this project.

REFERENCES

1. Renno, G.; Chen, D.; Zhang, Q. X.; Gomila, R. M.; Frontera, A.; Sakai, N.; Ward, T. R.; Matile, S. Pnictogen-Bonding Enzymes. *Angew. Chem. Int. Ed. Engl.* **2024,** 63 (45), e202411347.

2. Bering, L.; Craven, E. J.; Sowerby Thomas, S. A.; Shepherd, S. A.; Micklefield, J. Merging enzymes with chemocatalysis for amide bond synthesis. *Nat. Commun.* **2022,** *13* (1), 380.

3. Gergel, S.; Soler, J.; Klein, A.; Schulke, H. K.; Hauer, B.; Borras, G. M.; Hammer, C. S. Engineered cytochrome P450 for direct arylalkene-to-ketone oxidation via highly reactive carbocation intermediates. *Nat. Cat.* **2023**, *6*, 606-617.

4. Bolivar, J. M.; Woodley, J. M.; Fernandez-Lafuente, R. Is enzyme immobilization a mature discipline? Some critical considerations to capitalize on the benefits of immobilization. *Chem. Soc. Rev.* **2022,** *51* (15), 6251-6290.

5. Sheldon, R. A.; Basso, A.; Brady, D., New frontiers in enzyme immobilisation: robust biocatalysts for a circular bio-based economy. *Chem. Soc. Rev.* **2021,** *50* (10), 5850-5862.

6. Imam, H. T.; Marr, P. C.; Marr, A. C. Enzyme Entrapment, Biocatalyst Immobilization without Covalent Attachment. *Green Chem.* **2021**, *23* (14), 4980–5005.

7. Lopez, I. L.; Sanchez-Costa, M.; Orrego, A. H.; Zeballos, N.; Roura Padrosa, D.; Lopez-Gallego, F. Microtiter Plate Immobilization Screening for Prototyping Heterogeneous Enzyme Cascades. *Angew. Chem. Int. Ed. Engl.* **2024,** *63* (35), e202407411.

8. Thompson, L. A.; Rowbotham, J. S.; Nicholson, J. H.; Ramirez, M. A.; Zor, C.; Reeve, H. A.; Grobert, N.; Vincent, K. A. Rapid, Heterogeneous Biocatalytic Hydrogenation and Deuteration in a Continuous Flow Reactor. *ChemCatChem* **2020,** *12* (15), 3913-3918.

9. Zhang, W.; Huang, W.; Tan, J.; Guo, Q.; Wu, B. Heterogeneous catalysis mediated by light, electricity and enzyme via machine learning: Paradigms, applications and prospects. *Chemosphere* **2022,** *308*, 136447.

10. Wang, X.; Yiu, H. H. P. Heterogeneous Catalysis Mediated Cofactor NADH Regeneration for Enzymatic Reduction. *ACS Catal.* **2016,** *6* (3), 1880-1886.

11. Poznansky, B.; Thompson, L. A.; Warren, S. A.; Reeve, H. A.; Vincent, K. A. Carbon as a Simple Support for Redox Biocatalysis in Continuous Flow. *Org. Process Res. Dev.* **2020,** *24* (10), 2281-2287.

12. Verma, N. K.; Raghav, N. Comparative study of covalent and hydrophobic interactions for alpha-amylase immobilization on cellulose derivatives. *Int. J. Biol. Macromol.* **2021,** *174*, 134-143.

13. Neupane, S.; Patnode, K.; Li, H.; Baryeh, K.; Liu, G.; Hu, J.; Chen, B.; Pan, Y.; Yang, Z. Enhancing Enzyme Immobilization on Carbon Nanotubes via Metal-Organic Frameworks for Large-Substrate Biocatalysis. *ACS Appl. Mater. Interfaces* **2019,** *11* (12), 12133-12141.

14. Zhang, Z.; Gao, L.; Boes, A.; Bajer, B.; Stotz, J.; Apitius, L.; Jakob, F.; Schneider, E. S.; Sperling, E.; Held, M.; Emmler, T.; Schwaneberg, U.; Abetz, V. An enzymatic continuous-flow reactor based on a pore-size matching nano- and isoporous block copolymer membrane. *Nat. Commun.* **2024,** *15* (1), 3308.

15. Gupta, M.; Bandyopadhyay, A.; Sinha, S. K.; Chahar, S.; Samanta, A.; Mondal, S.; Bhattacharyya, S.; Datta, S. Heterogeneous Biocatalysis by Magnetic Nanoparticle Immobilized Biomass-Degrading Enzymes Derived from Microbial Cultures. *J. Mater. Chem. B* **2025**.

16. Deon, M.; Carminatti Ricardi, N.; Carvalho de Andrade, R.; Hertz, P. F.; Nicolodi, S.; Costa, T. M. H.; Bussamara, R.; Benvenutti, E. V.; de Menezes, E. W. Designing a Support for Lipase Immobilization Based On Magnetic, Hydrophobic, and Mesoporous Silica. *Langmuir* **2020,** *36* (34), 10147-10155.

17. Luckarift, H. R.; Spain, J. C.; Naik, R. R.; Stone, M. O. Enzyme immobilization in a biomimetic silica support. *Nat. Biotechnol.* **2004,** *22* (2), 211-3.

18. Lykourinou, V.; Chen, Y.; Wang, X. S.; Meng, L.; Hoang, T.; Ming, L. J.; Musselman, R. L.; Ma, S. Immobilization of MP-11 into a mesoporous metal-organic framework, MP-11@mesoMOF: a new platform for enzymatic catalysis. *J. Am. Chem. Soc.* **2011,** *133* (27), 10382-5.

19. Zheng, Y.; Zhang, S.; Guo, J.; Shi, R.; Yu, J.; Li, K.; Li, N.; Zhang, Z.; Chen, Y. Green and Scalable Fabrication of High-Performance Biocatalysts Using Covalent Organic Frameworks as Enzyme Carriers. *Angew. Chem. Int. Ed. Engl.* **2022,** *61* (39), e202208744.

20. Cote, A. P.; Benin, A. I.; Ockwig, N. W.; O'Keeffe, M.; Matzger, A. J.; Yaghi, O. M. Porous, crystalline, covalent organic frameworks. *Science* **2005,** *310*, 1166-1170.

21. Han, X.; Zhou, Z.; Wang, K.; Zheng, Z.; Neumann, S. E.; Zhang, H.; Ma, T.; Yaghi, O. M. Crystalline Polyphenylene Covalent Organic Frameworks. *J. Am. Chem. Soc.* **2024,** *146* (1), 89-94.

22. Zhou, Z.; Ma, T.; Zhang, H.; Chheda, S.; Li, H.; Wang, K.; Ehrling, S.; Giovine, R.; Li, C.; Alawadhi, A. H.; Abduljawad, M. M.; Alawad, M. O.; Gagliardi, L.; Sauer, J.; Yaghi, O. M. Carbon dioxide capture from open air using covalent organic frameworks. *Nature* **2024,** *635* (8037), 96-101.

23. Zhang, Z.; Meng, F.; Chi, X.; Jiao, Y.; Xue, B.; Li, X.; Zhang, F. Diketopyrrolopyrrole-Activated Dynamic Condensation Approach to Narrow-Band Gap Vinylene-Linked Covalent Organic Frameworks. *Angew. Chem. Int. Ed. Engl.* **2024**, e202417805.

24. Kumar Mahato, A.; Pal, S.; Dey, K.; Reja, A.; Paul, S.; Shelke, A.; Ajithkumar, T. G.; Das, D.; Banerjee, R., Covalent Organic Framework Cladding on Peptide-Amphiphile-Based Biomimetic Catalysts. *J. Am. Chem. Soc.* **2023,** *145* (23), 12793-12801.

25. Wang, K. Y.; Zhang, J.; Hsu, Y. C.; Lin, H.; Han, Z.; Pang, J. Yang, Z.; Liang, R. R.; Shi, W.; Zhou, H. C. Bioinspired Framework Catalysts: From Enzyme Immobilization to Biomimetic Catalysis. *Chem. Rev.* **2023,** *123* (9), 5347-5420.

26. Fairchild, D. C.; Hossain, M. I.; Cordova, J.; Glover, T. G.; Uribe-Romo, F. J., Steric and Electronic Effects on the Interaction of Xe and Kr with Functionalized Zirconia Metal–Organic Frameworks. *ACS mater. lett.* **2021,** *3* (5), 504-510.

27. Paul, S.; Gupta, M.; Kumar Mahato, A.; Karak, S.; Basak, A.; Datta, S.; Banerjee, R. Covalent Organic Frameworks for the Purification of Recombinant Enzymes and Heterogeneous Biocatalysis. *J. Am. Chem. Soc.* **2024,** *146* (1), 858-867.

28. Karak, S.; Singh, H.; Biswas, A.; Paul, S.; Manna, S.; Nishiyama, Y.; Pathak, B.; Banerjee, A.; Banerjee, R. Lithiophilic Dibenzamide Linkages to Impart Lithium Storage Capacity in Porous Polybenzamides. *J. Am. Chem. Soc.* **2024,** *146* (29), 20183-20192.

29. Liu, Y.; Chen, Z.; Wang, Z.; Lv, Y. Boosted Enzyme Activity via Encapsulation within Metal–Organic Frameworks with

Pores Matching Enzyme Size and Shape. *Adv. Sci.* **2024**, *11* (21), 2309243.

30. Qiao, S.; Jin, H.; Zuo, A.; Chen, Y. Integration of Enzyme and Covalent Organic Frameworks: From Rational Design to Applications. *Acc. Chem. Res.* **2024,** *57* (1), 93-105.

31. Zhang, Y.; Xing, C.; Mu, Z.; Niu, Z.; Feng, X.; Zhang, Y.; Wang, B. Harnessing Self-Repairing and Crystallization Processes for Effective Enzyme Encapsulation in Covalent Organic Frameworks. *J. Am. Chem. Soc.* **2023,** *145* (24), 13469-13475.

32. Liu, H.; Zhou, Y.; Guo, J.; Feng, R.; Hu, G.; Pang, J.; Chen, Y.; Terasaki, O.; Bu, X. H. Reticular Synthesis of Highly Crystalline Three-Dimensional Mesoporous Covalent-Organic Frameworks for Lipase Inclusion. *J. Am. Chem. Soc.* **2023,** *145* (42), 23227-23237.

33. Xing, C.; Mei, P.; Mu, Z.; Li, B.; Feng, X.; Zhang, Y.; Wang, B. Enhancing Enzyme Activity by the Modulation of Covalent Interactions in the Confined Channels of Covalent Organic Frameworks. *Angew. Chem. Int. Ed. Engl.* **2022,** *61* (21), e202201378.

34. Akpinar, I.; Wang, X.; Fahy, K.; Sha, F.; Yang, S.; Kwon, T. W.; Das, P. J.; Islamoglu, T.; Farha, O. K.; Stoddart, J. F., Biomimetic Mineralization of Large Enzymes Utilizing a Stable Zirconium-Based Metal-Organic Frameworks. *J. Am. Chem. Soc.* **2024,** *146* (8), 5108-5117.

35. Guo, L.; He, R.; Chen, G.; Yang, H.; Kou, X.; Huang, W.; Gao, R.; Huang, S.; Huang, S.; Zhu, F.; Ouyang, G., A Synergetic Pore Compartmentalization and Hydrophobization Strategy for Synchronously Boosting the Stability and Activity of Enzyme. *J. Am. Chem. Soc.* **2024,** *146* (25), 17189-17200.

36. Chao, H.; Zhou, Z.; He, W.; Li, M.; Yuan, X.; Su, P.; Song, J.; Yang, Y. Template-Free In Situ Encapsulation of Enzymes in Hollow Covalent Organic Framework Capsules for the Electrochemical Analysis of Biomarkers. *ACS Appl. Mater. Interfaces* **2022,** *14* (18), 20641-20651.

37. Feng, M.; Niu, Z.; Xing, C.; Jin, Y.; Feng, X.; Zhang, Y.; Wang, B. Covalent Organic Framework Based Crosslinked Porous Microcapsules for Enzymatic Catalysis. *Angew. Chem.* **2023**, *135* (33), e202306621.

38. Zhang, S.; Zheng, Y.; An, H.; Aguila, B.; Yang, C.; Dong, Y.; Xie, W.; Cheng, P.; Zhang, Z.; Chen, Y.; Ma, S. Covalent Organic Frameworks with Chirality Enriched by Biomolecules for Efficient Chiral Separation. *Angew. Chem. Int. Ed.* **2018**, *57* (51), 16754–16759.

39. Liu, Y.; Wang, Y.; Li, H.; Guan, X.; Zhu, L.; Xue, M.; Yan, Y.; Valtchev, V.; Qiu, S.; Fang, Q. Ambient Aqueous-Phase Synthesis of Covalent Organic Frameworks for Degradation of Organic Pollutants. *Chem. Sci.* **2019**, *10* (46), 10815–10820.

40. Jin, C.; Li, N.; Lin, E.; Chen, X.; Wang, T.; Wang, Y.; Yang, M.; Liu, W.; Yu, J.; Zhang, Z.; Chen, Y. Enzyme Immobilization in Porphyrinic Covalent Organic Frameworks for Photoenzymatic Asymmetric Catalysis. *ACS Catal.* **2022**, *12* (14), 8259–8268.

41. Gao, R.; Kou, X.; Tong, L.; Li, Z. W.; Shen, Y.; He, R.; Guo, L.; Wang, H.; Ma, X.; Huang, S.; Chen, G.; Ouyang, G. Ionic Liquid-Mediated Dynamic Polymerization for Facile Aqueous-Phase Synthesis of Enzyme-Covalent Organic Framework Biocatalysts. *Angew. Chem. Int. Ed. Engl.* **2024,** *63* (8), e202319876.

42. Lin, S. W.; Lam, P. K.; Wu, C. T.; Su, K. H.; Sung, C. F.; Huang, S. R.; Chang, J. W.; Shih, O.; Yeh, Y. Q.; Vo, T. H.; Tsao, H. K.; Hsieh, H. T.; Jeng, U. S.; Shieh, F. K.; Yang, H. C. Decoding the Biomimetic Mineralization of Metal-Organic Frameworks in Water. *ACS Nano* **2024,** *18* (36), 25170-25182.

43. Möslein, A.F.; Gutiérrez, M.; Cohen, B.; Tan, J.C. Near-field infrared nanospectroscopy reveals guest confinement in metal-organic framework single crystals. *Nano Lett.* **2020,** *20*, 7446–7454.

44. More, Y.D.; Mollick S., Saurabh, S., Fajal S., Tricarico M., Dutta S., Shirolkar, M. M.; Mandal, W.; Tan, J.C.; Ghosh, S.K. Nanotrap Grafted Anionic MOF for Superior Uranium Extraction from Seawater. *Small* **2024,** *20*, 2302014.

45. Krylov, A.; Vtyurin, A.; Petkov, P.; Senkovska, I.; Maliuta, M.; Bon, V.; Heine, T.; Kaskel, S.; Slyusareva, E. Raman Spectroscopy Studies of the Terahertz Vibrational Modes of a DUT-8 (Ni) Metal-Organic Framework. *Phys. Chem. Chem. Phys.* **2017,** *19*, 32099– 32104.

46. Guo, L.; Zhang, Q. Y.; Yu, Z.; Krishna, R.; Luo, F. Minute and Large-Scale Synthesis of Covalent-Organic Frameworks in Water at Room Temperature by a Two-Step Dissolution–Precipitation Method. *Chem. Mat.* **2023,** *35* (14), 5648-5656.

47. Gudiksen, K. L., Gitlin, I., Whitesides, G. M. Differentiation of proteins based on characteristic patterns of association and denaturation in solutions of SDS. *Proc. Natl. Acad. Sci. U. S. A.* **2006**, *103*, 7968–7972.

48. Liang, W.; Xu, H.; Carraro, F.; Maddigan, N. K.; Li, Q.; Bell, S. G.; Huang, D. M.; Tarzia, A.; Solomon, M. B.; Amenitsch, H.; Vaccari, L.; Sumby, C. J.; Falcaro, P.; Doonan, C. J. Enhanced Activity of Enzymes Encapsulated in Hydrophilic Metal–Organic Frameworks. *J. Am. Chem. Soc.* **2019**, *141* (6), 2348–2355.

49. Paul, S.; Gupta, M.; Dey, K.; Mahato, A.; Bag, S.; Torris, A.; Gowd, E.B.; Sajid, H.; Addicoat, M.; Datta, S.; Banerjee, R. Hierarchical covalent organic framework-foam for multi-enzyme tandem catalysis. *Chem. Sci.* **2023**, *14*, 6643–6653.

Table of Contents

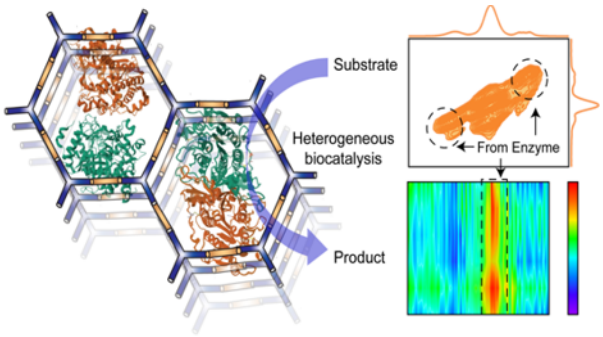
Substrate
Heterogeneous
biocatalysis
Product
From Enzyme